African Journal of Pure & Applied Sciences

ISSN: 2710-0758
DOI: https://doi.org/10.33886/ajpas.v5i2.569

Journal homepage: http://journal.ku.ac.ke/index.php/AJPAS

Research Article Open Access

Effect of reaction temperature on structural growth, optical, and electrical properties of Cu-doped ZnS thin film synthesized via spray pyrolysis technique

Bogere Sula[1], Munji Mathew & Ochoo Lawrence

[1]Department of Physics, Kenyatta University

[1*]Corresponding author email address munji.mathew@ku.ac.ke

Received 2nd July, 2024: Accepted 11th November 2024; Published online: 20th December 2024

How to Cite:

Bogere , S., Munji , M., & Ochoo , L. Effect of reaction temperature on structural growth, optical, and electrical properties of Cu-doped ZnS thin film synthesized via spray pyrolysis technique. *African Journal of Pure and Applied Sciences, 5(2),* 50–61. https://doi.org/10.33886/ajpas.v5i2.569

ABSTRACT

Cu-doped ZnS (CuZnS) thin films were deposited via chemical spray pyrolysis, and the effect of substrate temperature on their structural, optical, and electrical properties was investigated. XRD and Raman analysis were conducted to study the structural properties of the grown CuZnS thin films and the analysis revealed a moderate polycrystalline structure with mixed phase of hexagonal and less cubic phases. The strain of about 3.29 × 10^{-2} and the density of dislocation of about 8.436 × 10^{16} lines/m^2 were found at 410 °C. Double bandgaps of about 3.4 eV and 3.1 eV were obtained from Tauc's plots of the utilized substrate temperatures. From the modified Scherrer equation, crystallite sizes of about 4.427 nm and 3.443 nm at the substrate temperatures of 380 °C and 410 °C respectively were obtained. The structural analysis and the obtained Urbach energy showed the presence of imperfections and residue stresses in the grown CuZnS thin films which revealed the unattained thermodynamic stability in the phase transitioning to a dominant hexagonal phase in grown CuZnS even at 410 °C. The analysis results indicated that CuZnS thin films grown via spray pyrolysis for optoelectronic applications including UV photodetectors and LEDs, are best deposited at a substrate temperature above 410 °C and under sufficiently controlled surrounding environment within the enclosure of the machine to avoid unnecessary oxidation at elevated temperatures.

Keywords: CuZnS, substrate temperature, Phase transition, Thermodynamic stability

INTRODUCTION

Transparent semiconductors extend beyond oxides, encompassing several classes of non-oxide semiconductors. Among these are the group VI chalcogenide (Ch) semiconductors, including binary II-VI MCh semiconductors (e.g., ZnS, CdS, $Zn_xCd_{1-x}S$). Binary bivalent metal chalcogenides $M^{2+}Ch^{2-}$ (Ch = S, Se, Te), primarily form the simplest class of wide bandgap (WBG) Ch semiconductors (WBGSs show band-to-band absorption edges larger than 2 eV below 620 nm wavelengths) [1, 2]. In this study, we will use semiconducting ternary compound chalcogenide (Ch) thin films, which have garnered considerable attention from researchers in recent decades due to their wide-ranging applications in science and technology. These applications include solar cells, LEDs, sensors, and various electronic and optical devices that involve transparent contacts, p–n junctions, and thin-film transistors [3, 4, 5]. Additionally, chalcogenides were chosen for this study because they are more amenable to p-type doping, attributed to their higher-lying p-derived valence bands and lower ionization energies [1, 2]. ZnS, with a bandgap energy of $E_g \approx 3.7$ eV, is known for its n-type characteristics, high optical transparency, conductivity potential, and low toxicity. It will be tailored to exhibit p-type conductivity through appropriate doping with Cu, while maintaining its transparency [6, 7, 8]. Like ZnO, ZnS crystallizes in cubic zincblende (ZB) or hexagonal wurtzite (WZ) phases, both with wide direct band gaps. Incorporating Cu^+ into ZnS will create copper vacancies, enabling p-type conduction [6, 7]. Alloys i.e. $Cu_xZn_{1-x}S$, and phase-separated composites i.e. Cu_xS: ZnS past the solubility limit of Cu, formed from these

binaries, offer tunable optoelectronic properties and are highly explored in the space of transparent conducting oxides [1, 2]. The initial stoichiometry (Cu+Zn):S:1:1 will influence the composition of the final CuZnS (CZS) thin film thus, Cu-doped ZnS films with over 5 at.% Cu will exhibit p-type conductivity due to copper's +1 state [7].

Several chemical, and physical vapour deposition techniques have been employed to grow Cu-doped ZnS nanostructures like thin films have been reported including chemical bath deposition [3, 4, 9, 5], sol-gel [10], hydrothermal method [11], spray pyrolysis [12, 13, 14, 7, 15, 8], pulse laser [16], photochemical deposition [17, 18], RF magnetron sputtering technique [19], and successive ionic layer absorption technique (SILAR) [3]. Among the various growth techniques, spray pyrolysis, which will be employed in this study, is one of the most prominent methods used for growing Cu-doped ZnS nanostructure materials, including thin films. Its popularity stems from its affordability, and effectiveness, both in terms of the chemicals used and the simplicity of assembling the deposition apparatus.

First of all, in this study, we deposited thin films at substrate temperatures of 340 °C, 360 °C, 380 °C, 390 °C, 400 °C, 410 °C, 420 °C, 440 °C, and 460 °C under other optimized parameters. During optical optimization using average absorbance, an unusual behaviour was revealed between 380 °C and 410 °C as shown in Figure 1, where a slight decrease in absorbance was observed, contrary to the expected increase with rising substrate temperature. This triggered curiosity and the findings were first compared with Emegha *et al.* [20], who reported the gradual formation of additional peaks as deposition temperature increased from 370 °C to 400 °C, as well as a notable reduction in grain size within this range. Additionally, a gradual decrease in XRD peak intensity beyond 400 °C was documented. One of the two conduction mechanisms with a low activation energy was also reported to exist between the temperatures of 370 °C to about 430 ° [21]. This prompted us to focus on the structural processes that might explain the observed unexpected decrease in optical absorbance near 400 °C in light of Emegha *et al.*'s findings.

The growth of CuZnS thin films exhibits a combination of hexagonal and cubic phases other than individual phases, at a certain reaction temperature range. This mixed phase is reported to be linked to a structural phenomenon influenced by a reaction temperature around 400 °C [22, 7, 23]. Krishna and Mahesha used a temperature of about 420 °C to deposit the CuZnS thin films by spray pyrolysis technique though not much was discussed about the region of choice of the reaction temperature [7, 15]. Any structural changes occurring near this temperature are crucial in selecting the right reaction temperature for producing high-quality CuZnS thin films through temperature-dependent deposition methods including spray pyrolysis.

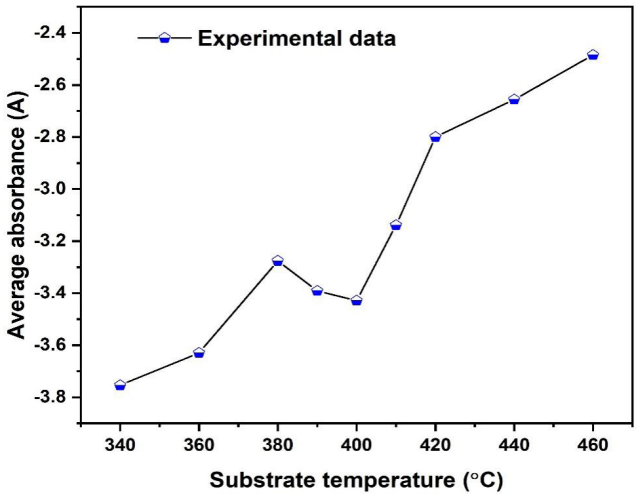

Figure 1: Average absorbance plot for the synthesized thin films of CuZnS at different substrate temperatures in the NUV, and UV-visible regions.

With the asserted motivation, this research study discusses the structural processes that occur near 400 °C reaction temperature, and their effects, particularly on the optical properties of the synthesised alloy of CuZnS thin films and the influence on the choice of substrate temperature for Photovoltaic applications including UV photodetection and LED

EXPERIMENTAL PROCEDURES

The p-Cu-doped ZnS thin film samples used in this study were grown via a locally assembled chemical spray pyrolysis technique. Firstly, the growth parameters were optimized and then used to deposit the uniform thin films at 380 °C, and 410 °C. The estimated thicknesses by the Alpa-step profiler were about 841.67 nm and 755.33 nm at 380 °C, and 410 °C surface temperatures respectively. The film thickness was controlled by using an optimal spray rate of 5 ml/min, spray pressure of 30 PSI, deposition time of 3 minutes, and substrate-to-nozzle distance of 26 cm. These parameters, especially the spray time, were significantly influenced by the configuration of the assembled instrument. Prior to the film growth, cleaning of the glass substrates was thoroughly performed firstly, with ethanol followed by acetone for 10 minutes each, and a 3-times rinse in an ultra-sonicator with distilled water for 15 minutes. After drying at room temperature, they were then transferred to a UV Ozone cleaner for 10 minutes for the final cleaning. The Precursor solution of analytic grade reagents (AR/ACS) of copper chloride dehydrate ($CuCl.2H_2O$), zinc chloride ($ZnCl_2$), and thiourea ($CS(NH_2)_2$)

in 50 ml of distilled water was prepared to yield 2.45 g of CuZnS. The Cu atomic doping percentage, at. % was optimized from 0 at. % to 24 at. % to determine the doping level that achieves low electrical sheet resistance. Graphical analysis as shown in Figure 2 and values listed in Table 1 showed that electrical sheet Resistance decreased with a higher Cu atomic doping percentage. It was observed that at 24 at. % Cu doping in ZnS, aggregation occurred immediately upon mixing the reactants, leading to the appearance of a white-like phase spreading throughout the mixture. This resulted in a highly viscous, phase-separated mixture (surface aggregation due to excessive Cu doping in the ZnS matrix) that could not be sprayed. The choice of 16 at. % was primarily aimed at achieving high conductivity, with 20 at. % omitted because 16 at. % could provide higher charge carrier mobility, owing to the slightly lower doping level, according to the relationship between electrical conductivity and charge carrier mobility. Additionally, the choice was influenced by reports from Krishna and Mahesha [7, 15], who noted higher charge carrier mobility at 15 at. % Cu doping compared to 20 at. %. Thus, the Cu doping percentage was maintained at 16 at. % and the reaction temperature was varied near 400 °C in comparison to Krishna and Mahesha., and Emegha *et al.* [7, 15, 20, 21]. The mass of CuCl. $2H_2O$ required to contribute 16 at. % of Cu in order to yield 2.45 g of CuZnS alloy was stirred for 10 minutes.

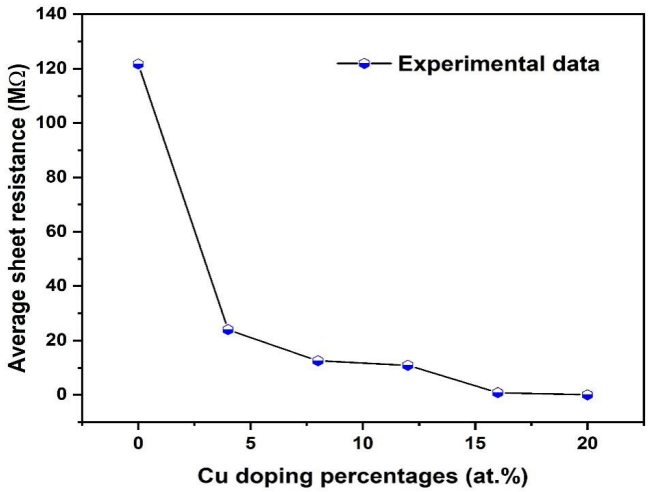

Figure 2: A line plot of Cu doping percentages against average sheet resistance of CuZnS thin film grown at about 420 °C.

The mass of $ZnCl_2$ on the remaining atomic percentage ratio from that of Cu was added to the resultant solution and stirred for 15 minutes. The mass of $CS(NH_2)_2$ required to yield the 2.45 g of CuZnS in the stack solution was added, and further stirring of the resultant for 55 minutes was performed to obtain a homogeneous solution. CuZnS is generated as shown in Eq. (1) [7, 15]

$$Zn_{1-x}Cl_2 + CuCl_2 \cdot 2H_2O + 2CS(NH_2)_2 + 2H_2O \rightarrow Cu_xZn_{1-x}S + 4HCl + 4NH_3 + 2CO_2 \quad (1)$$

The contributed mass of Cu (m_{Cu}) in the 2.45 g of CuZnS was calculated from Eq. (2), where m_T denotes the total mass of the constituent elements in CuZnS at the chosen Cu doping atomic percentage.

$$m_{Cu} = \left(\frac{m_{Cu_x}}{m_T} \times 2.56\ g\right) \quad (2)$$

The mass of the reactant, CuCl. $2H_2O$ (CCD) entailed to yield the mass of the constituent element of Cu_x in the CuZnS was calculated as shown in Eq. (3), where m.m represents the molecular mass.

$$m_{CCD\,Cu_x} = \left(\frac{m.m_{CCD}}{m.m_{Cu}} \times m_{Cu}\right) g \quad (3)$$

Similarly, the masses of zinc chloride and thiourea were calculated as shown by Eq. (3). Finally, the total mass of the reactants in 50 ml of distilled water was calculated, and thus, the mass of each reactant required in 50 ml was found.

Optical characterization was performed with a Solid Spec-3700 DUV spectrophotometer. The XRD spectra to investigate the structure were recorded using a Thermo Scientific ARL EQUINOX 100 X-Ray Diffractometer with Cu K_α:1.504 Å. The elemental composition from EDX spectra was recorded from EDX-800HS SHIMADZU energy dispersive X-Ray spectrometer at a voltage of 50 kV of an X-ray tube. Raman spectra analysis studies were performed with STR Raman comprising of OLYMPUS ST BX51 confocal Raman optical microscope, and a Peltier cooled Charge coupled device (CCD) detector utilizing a 532 nm excitation source of the laser beam, and 600 grooves/mm diffraction grating. Thickness analysis was performed with an Alpha-step IQ surface profilometer, and the Keithley 2400 source meter unit with the four-point probe was used for electrical characterization.

RESULTS AND DISCUSSION

Structural study

The XRD patterns of Cu-doped ZnS thin films at 16 at. % Cu doping with different substrate temperatures of 380 °C and 410 °C are shown in Figure 3. The XRD analysis was conducted in a 2θ scanning range of 20 ° - 65 ° and the spectra were compared against the XRD results of Cu-doped ZnS thin films [24, 22, 7, 14, 23, 25, 20, 8, 5]. A main peak is observed at 31.18 ° for the grown thin film at 410 °C while at 25.50 ° for that deposited at 380 °C. The intensity increased for the peaks at 2θ = 31.18 ° (100)/(101), 34.64 ° (200)/(002), 52.27 ° (103)/(1012) and 59.31(311)/(004) reflection planes. However, it decreased for the peaks of 25.50 ° (008)/(002)/ (100), 39.77 ° (400)

and 42.23 ° (102) respectively. The Gaussian fit reports an additional peak, at 2θ = 61.75 ° (311) in the thin film spectrum of 410 °C. The intensity for the peak of 25.50 ° decreased while increased for the peaks of 31.18 °, and 34.64 ° upon increasing the substrate temperature from 380 °C to 410 °C.

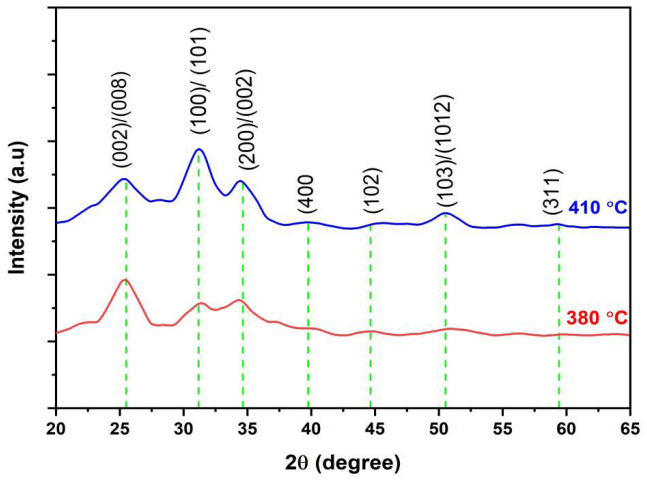

Figure 3: XRD spectra of CuZnS thin film sprayed at 380 °, and 410 ° substrate temperatures.

The broadening of peaks observed in both XRD spectra revealed the less polycrystallity degree possessed by the deposited thin films at both substrate temperatures [26, 20]. The slight increase in intensity and the number of peaks in the spectra of the thin films deposited at a reaction temperature of 410°C is attributed to a modest increase in crystallinity, unveiled by the estimated degree of crystallinity, which rose from 20.01 % to 30.29 % upon raising substrate temperature. The peak observed at 25.5 ° is associated with the hexagonal ZnS peaks (002)/(008)/(100), indexed according to the wurtzite structure of ZnS, as per standard JCPDS cards (JCPDS card No o-8000007, JCPDS # 80-0007 & 06-0464, & JCPDS-00-036-1450) [27, 25, 8, 5]. The major peak at 2θ = 31.18 °, and 34.64 ° in the 410 °C spectrum corresponds to the peak for hexagonal wurtzite CuZnO [7, 28]. This aligns with the observed reduction in thin film thickness as the reaction temperature increased from 380 °C to 410 °C, suggesting a decrease in ZnS content within the synthesized film [8]. The corresponding minor peaks might be Cu-related sulphide or oxide peaks, of ZnO, or an alloy of CuZnO. The peaks at 39.77 ° and 59.31 ° correspond to the cubic phase of ZnS thin film with a sphalerite structure (JCPDS card 80-0020, JCPDS card 72-0163, JCPDS 050566, JCPDS 36-1450), while the peak at 52.27 ° corresponds to the hexagonal phase of CuZnS, consistent with the standard JCPDS cards (JCPDS card 72-0163, JCPDS card No o-8000007) [24, 29, 22, 30, 25, 21]. The minor addition peak at 61.75 ° might be of a varying valency of copper related to sulphur [7]. The observed changes in results of the spectrum of the thin film at 410 °C compared to that at 380 ° might be attributed to the transformation to the dominant hexagonal phase in the matrix [22, 7, 23]. However, increased levels of oxidation have been observed upon increasing the substrate temperature to 410 °C which might stem from the sulfur deficiency due to the considered atomic ratio in CuZnS [7]. Additionally, some of the oxidation may be attributed to insufficient control of the surrounding environment within the machine's enclosure particularly at the elevated reaction temperature of 410 °C, which likely facilitated some interaction between the surroundings and the grown film.

The crystallite sizes in the films grown at 380 °C and 410 °C were calculated using the intercept of the modified Scherrer equation, Eq. (5), as plotted in fig. 4(a) and fig. 4(b). The modified Scherrer equation, Eq. (5), is derived from the Debye-Scherrer equation, Eq. (4) [31].

$$D_{hkl} = \frac{k\lambda}{\beta \cos\theta} \quad (4)$$

$$\ln\beta = \ln\frac{1}{} \quad (5)$$

The crystallite size D of about 4.427 nm for the ZnS:Cu thin film deposited at 380 °C, and D of 3.443 nm at 410 °C were determined. The broader peaks in the XRD spectra agree with the estimated grain sizes that the synthesised thin films have small crystallites. The small sizes of the grains at both reaction temperatures likely linked to unattained thermodynamic stability and observed oxidation besides the slight reduction of the crystallite size on raising the temperature.

The dislocation density (δ), and strain (ε) present in the deposited thin films were determined using Eq. (6), and Eq. (7) respectively [5, 32].

$$\delta = \frac{1}{(D_{hkl})^2} \quad (6)$$

$$\varepsilon = \frac{\beta}{4\tan\theta} \quad (7)$$

The dislocation density in the grown thin films increased upon raising the temperature to 410 °C, as shown in Table 2, while the microstrain decreased with the increase in substrate temperature to 410 °C as shown in Table 3. The increase in dislocation density probably is attributed to ZnS:Cu thin film not having attained the thermodynamic stability in the phase transitioning to a properly mixed phase of Cubic and hexagonal phases as expected in the CuZnS lattice and moreover, linked to some revealed unnecessary

oxidation. The high overall microstrain obtained might be due to the residue stresses likely present in the grown films. It is from the phases having a close-by free energy required for the formation [22, 7, 23]

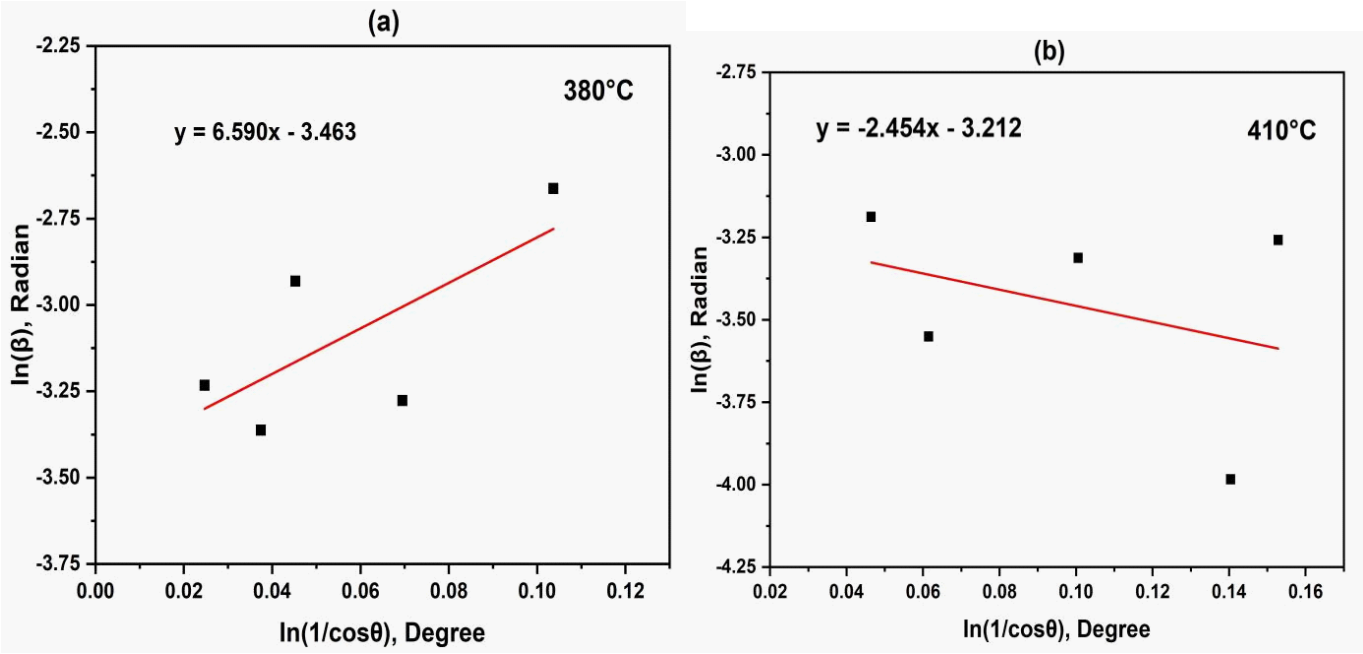

Figure 4: Linear plot of the Modified Scherrer equation for CuZnS thin film sprayed at 410 °, 380 ° substrate temperatures.

Raman Analysis

The Raman spectra in Figure 5 represent the Cu-doped ZnS thin films at maintained Cu doping of 16 at. % synthesized at 380 °C and 410 °C. Both chosen reaction temperatures are close to the most commonly reported reaction temperature of 400 °C regarding the crystallinity and formation of the alloy of CuZnS [14, 20].

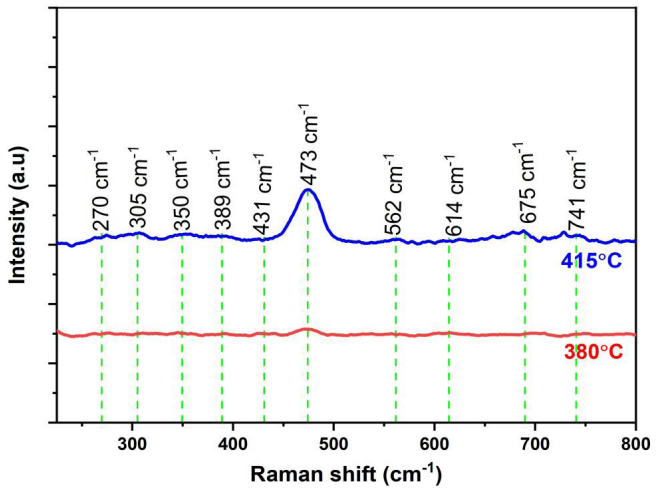

Figure 5: Raman spectra of CuZnS thin film sprayed at 380 ° and 410 ° substrate temperatures.

Raman spectroscopy was conducted for further structural details from analysis of the vibration modes in the spectra of grown thin films. The interpretation stems from the group theoretical analysis equation Eq. (8) for Raman-active phonons.

$$\Gamma_{opt} = A_1(Z) + 2B_1 + E_1(x,y) + 2E_2 \quad (8)$$

Γ_{opt} depicts the optical phonon modes, B_1 modes exhibit no observation on both spectroscopes (optically inactive), and E_2 is non-polar thus solely Raman active. A_1 and E_1 are polar and therefore active on IR and Raman spectroscopes. The analysis is based on the Raman scattering phenomena and the symmetry attributes of phonons in the crystal lattice [33, 34, 35, 36, 22, 14]. Raman peak fitting was conducted using Lorentzian fit in OriginPro 2018 software. Table 4 shows the observed Raman peaks at the sprayed substrate temperatures. The peak at 270 cm^{-1} corresponds to the E_1TO mode of ZnS which indicates the mixed phase of both cubic and hexagonal phases in the synthesised thin films of Cu-doped ZnS as compared to the reports about the comprehensive study of zinc blende and wurtzite ZnS by Brafman and Mitra., and Cheng *et al.* [33, 34, 35, 36, 22, 7, 8]. The peak at 305 cm^{-1} related to that at 317 cm^{-1} corresponds to the phonon density of states peak at 307 cm^{-1} (surface optical phonon mode) along X-W-L since it exists between the TO and LO modes, and it is attributed to the induced surface imperfections (surface vibration) in the matrix [36, 22, 7, 8]. The Raman peak at A_1 (LO) 350 cm^{-1} observed in the spectra at both temperatures was reported to also exist in hexagonal and cubic phases of ZnS [33, 34, 37, 35, 36, 22, 8]. The slight

shifting to higher wave numbers and the increase in the intensity indicates the dominance of the hexagonal over the cubic phase in the lattice of ZnS: Cu thin films on raising the reaction temperature. However, some successive shifts in the peak positions upon raising the temperature might have stemmed from the imperfections and residue stresses due to raising the reaction temperature [23]. The peaks at 389 cm^{-1} and 400 cm^{-1} correspond to the A_1(TO), and E_1(TO) optical modes of the ZnO lattice [28, 33]. The peak at 431 cm^{-1} profoundly observed in the spectra of 380 ° C, corresponds to the [LO + TA] mode of hexagonal ZnS [8]. The broader peak at 473 cm^{-1} is ascribed to the stretching vibrational mode of S-S bonds with A_{1g} symmetry stemming from S_2 atoms situated at 4e sites, and corresponding to the valence one copper phase (Cu^+) [38, 39, 7, 23]. The peak noticed at 562 cm^{-1} corresponds to the E_1/A_1 (LO) mode of CuZnO [28, 7]. The peaks observed at 614 cm^{-1}, and 675 cm^{-1} correspond to the 2TO, and 2LO overtones that correspond to the points at L, and Γ respectively in the Brillouin zone (BZ) which might signify surface modifications from compressions or expansions possibly due to induced defects or are ascribed to overtone and combination scattering processes at relatively high densities of states (DOS) of two phonons [34, 35, 8]. However, the 614 cm^{-1} mode might alternatively, be revealing the Bg CuO reported by EDX analysis [28]. The peak at 741 cm^{-1} corresponds to the 2LO mode which may be due to the high 16 at. % doping concentration of Cu used since these are overtones or combinations of first-order Raman scattering LO and TO peaks [37, 8]. The observed Raman modes indicate the formation of ZnS and successful incorporation of Cu in the ZnS matrix, besides the observed increased oxidation depicted by some noticed Raman peaks upon raising the reaction temperature to 410 °C.

EDX analysis

The elemental composition analysis in the Cu-doped ZnS thin film synthesized at 410 °C shows the peaks of Zn, Cu and Sulphur as seen in fig. 6(a). Additionally, the results displayed in the report fig. 6(b) confirmed the presence of the individual elements Zn, Cu, S, and Cl. The intensity of the Zn peak was reported to be the highest, followed by Cu, and the sulphur, indicating its highest composition in grown film. The intensity of sulfur relative to Zn further indicated its deficiency, likely due to oxidation, as evidenced by the presence of ZnO and CuO reported in Table 5, which are likely components of CuZnO alloy, as revealed by XRD, Raman, and optical bandgap analyses. The ZnKα peaks and ZnKβ indicated that Zn had both L and M shell electron transitions to K shell electron vacancies respectively.

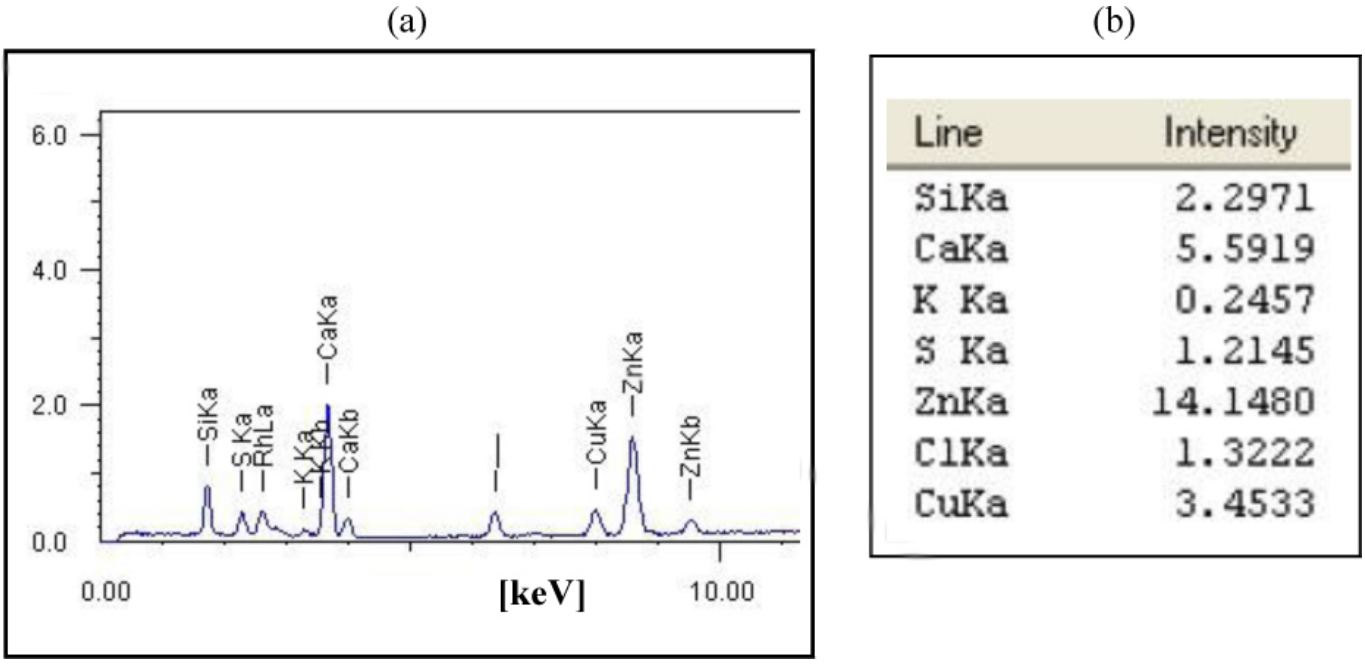

Figure 6: (a) EDX spectrum, and (b) EDX analysis report of the CuZnS thin film.

The reported peaks of Zn and sulphur signify the formation of the ZnS phase in the matrix. A notable peak of Cu is observed in the spectra, revealing copper incorporation in the phase. The additional report, as shown in Table 5, identified ZnO, CuO, and some contributions from SO_2, as the instrument only supported and reported binary oxides. Thus, binary sulfur compounds could not be detected or reported, even if present, unlike oxides. The ZnO, CuO, and SO_2 reported might be attributed to the surface oxidation which is in agreement with the XRD, and Raman analyses. However, some SO_2 is contributed by the glass substrate in addition to the reported SiO_2,

CaO, and K_2O as shown in the results column of Table 5. The Chloride reported by EDX probably might be from the product of HCl in the aqueous form generated during the reaction as seen in the reaction Eq. (1).

UV-Vis spectrophotometer analysis

The absorption spectra of 16 at. % Cu-doped ZnS thin films synthesized at 380 °C, and 410 °C in the wavelength range 200 - 850 nm are as shown in Figure 7. The absorption edges of the recorded spectra at 380 °C, and 410 °C surface temperatures are about 425 nm, and 450 nm respectively. From the spectra, it is observed that the absorbance values are high in the Near-ultraviolet (NUV), and substrate temperatures.

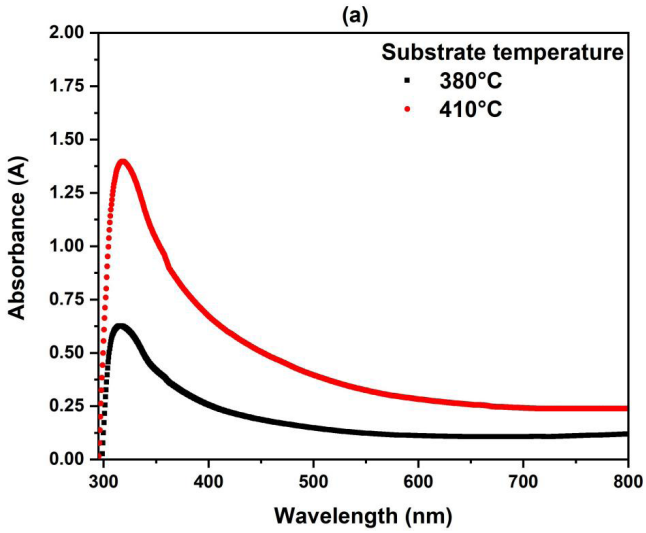

Figure 7: (a) Absorbance plot for the synthesized thin films of CuZnS at 380 °C, and 410 °C

UV-visible (blue UV) regions, however, it is higher for a thin film synthesized at 410 °C. The increase of absorption on raising the reaction temperature might be due to the observed improved crystallinity in XRD and Raman analyses which might have been due to a reduction in the imperfections and grain boundaries in the lattice [20]. It is also revealed by the observed decrease in the thin film thickness measured. It might also be ascribed to the observed dominance of the hexagonal over the cubic phase of the mixed phases observed in the structural analysis, which might be in addition to changes in the stoichiometry observed with sulfur deficiency attributed to oxidation on raising the substrate temperature to 410 °C. Changes in the stoichiometry, and the dominant phase might have differently influenced the optical absorption property of the deposited thin films [40, 22]. The obtained absorbance data was employed to determine the absorption coefficient (α) which is related to the incident photon energy in Tauc's plot relation Eq. (9), utilized to estimate the optical bandgaps of the synthesised CuZnS thin films [22, 25, 5].

$$(\alpha h\nu) = A(h\nu - E_g)^n \quad (9)$$

A is a constant which reveals the sharpness of the absorption edge (it is called the band edge sharpness associated with the order of crystallinity in the synthesized film), hν - incident photon energy (h - is the Plank's constant, ν - is the photon frequency), Eg - is the Bandgap energy, and n- reflects the nature of the band transition. The type of the band transition, n, can be ½, 3/2, 2, or 3 representing the direct allowed, direct forbidden, indirect allowed, or indirect forbidden transitions respectively [41, 42, 22].

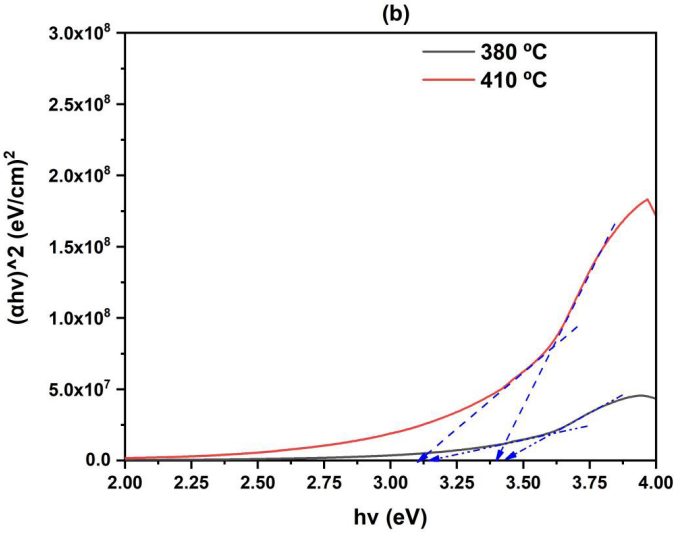

Figure 8: (a) Tauc's plots for the synthesized thin films of CuZnS at 380 °C, and 410 °C substrate temperatures.

E_g was determined by extrapolating the line portion of graphs of $(\alpha h\nu)^2$ versus incident photon energy hν to the energy axis as shown in Figure 8. From the indirect bandgap energies in Table 6 for thin films deposited at surface temperatures of 380 °C and 410 °C, it can be observed that each spectrum contains two bandgap energies. The bandgaps at 3.43 eV and 3.40 eV indicate ZnS formation, while the sub-bandgap energies of about 3.14 eV and 3.09 eV correspond to the bandgap of CuZnO, aligning with the XRD and Raman analyses [7] The sub-bandgaps are also in agreement with the 3.1 eV bandgap of 2 at. % CuZnO documented by Chen and Hsieh. [28]. Part of the formation may be attributed to oxidation due to inadequate control of the surrounding environment within the machine's enclosure mainly at the elevated reaction temperature of 410 °C, which likely promoted some interaction between the surroundings and the grown film. Urbach energies determined from Figure 9 as shown in Table 6 reveal a higher disorder in the CuZnS thin film synthesised at 410 °C, than at 380 °C which is in agreement with the high dislocation density obtained as shown in Table 2.

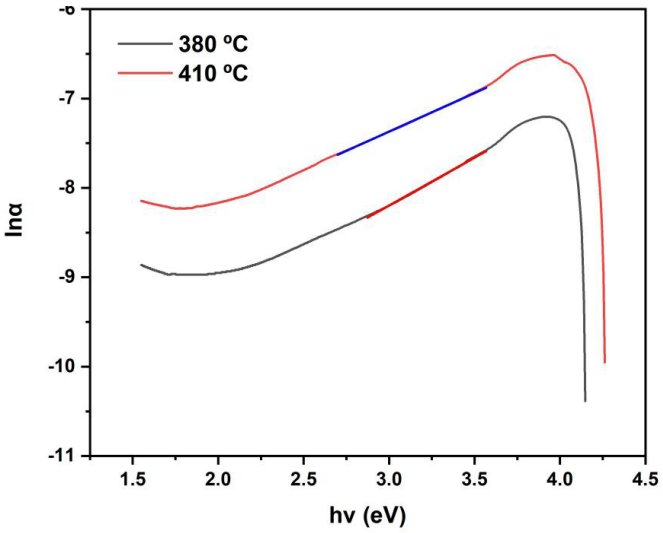

Figure 9: (a) Urbach energy plots for the synthesized thin films of CuZnS at 380 °C, and 410°C substrate temperatures.

This might be due to the thin film at 410 °C not having attained the thermodynamic stability in the phase transitioning, along with some unintended oxidation, as indicated by the XRD, Raman, EDX, and optical bandgap energy analyses. The observed band gaps are lower than the reported energy of the band gap, 3.7 eV of the bulk ZnS [22, 43, 30, 25]. It might be ascribed to the existing imperfections such as vacancies of sulfur due to oxidation, and induced zinc interstitials. The band gap energy can be altered by changes in the grain size, tensile and compression strains, dislocation density, and crystalline phases besides, the evaporation of sulfur and zinc that affect stoichiometry in the synthesised thin film [29, 22]. This might have reduced the energy of the band gap by raising the reaction temperature to 410 °C.

Measurement of conductivity

The sheet resistance of the thin films was measured using the Four-point probe technique with the four probes in a collinear symmetry connected to the Keithley 2400 source meter unit under the Van der Pauw configuration for measuring Voltage and Current [44, 45, 46, 47, 21]. The electrical conductivities in Table 7 revealed an increase in conductivity upon raising the substrate temperature indicating the semi-conductivity property exhibited by the synthesised CuZnS thin films. The increase in conductivity might be attributed to improved crystallinity as the reaction temperature was raised to 410 °C similar to the observed in XRD and Raman analyses, which might have reduced the imperfections in the lattice as compared to 380 °C. Furthermore, the enhanced conductivity may also be associated with the observed increase in the formation of CuZnO and Cu_2S as indicated by the XRD, Raman, and EDX analyses [7]. However, the increase was low in this region which might be attributed to hopping, and is in agreement with the previous report by Emegha *et al.*, [21].

CONCLUSION

Several peaks observed corresponded to the hexagonal phase over the cubic phase from the XRD, and Raman analyses. Increased intensity of the peaks and additional peaks from XRD, and Raman analysis upon raising the substrate temperature to 410 °C depict the enhanced crystallinity. The observed multiple peaks in the XRD spectra of the thin film synthesized at 410 °C indicated a polycrystalline structure of the thin film than at 380 °C, with about 30 % degree of crystallinity. However, the sharpness of the XRD and Raman peaks for the CuZnS thin film at 410 °C and the observed degree of crystallinity indicate the presence of defects and residue stresses in the structure. The observed decrease of the strain to $3.29 \times \varepsilon\ 10^{-2}$ and yet an increase in the density of dislocation to 8.436×10^{16} lines/m^2 probably depicts unattained thermodynamic stability in the phase transitioning to a dominant hexagonal phase in CuZnS. Additionally, this is likely due to increased oxidation at the elevated temperature of 410 °C, potentially leading to the formation of a CuZnO alloy, with CuO formed within the ZnO matrix upon incorporation of Cu, as revealed by XRD, Raman, EDX, and optical bandgap energy analyses. This explains the observed crystallite size decrease in this study which agrees with the reported significant reduction in the grain size upon raising the reaction temperature to 400 °C from 370 °C by Emegha *et al.* [20]. Because a phase change entails creating a clear boundary (interface) between the initial and final phases and involves the redistribution of atoms when the product phases have different compositions, the atomic movement takes time, indicating that a phase change typically does not happen simultaneously throughout the entire material [48]. Therefore, the results reveal that the CuZnS thin films to be synthesised via spray pyrolysis for optoelectronic applications including UV photon detectors and LEDs, are suitable to be deposited at a substrate temperature above 410 °C and within a carefully controlled surrounding environment in the machine's enclosure to prevent unnecessary oxidation at elevated temperatures. However, the reaction temperature should be below 430 °C due to the high activation energy required in the temperature region above 430 °C [21].

ACKNOWLEDGEMENTS

The authors are sincerely appreciative of the Inter-University Council for East Africa (IUCEA) in collaboration with the German Development Bank (KfW) for providing support to carry out this research.

Conflict of Interest

There is no clash of interests

Supporting Information

Not applicable

REFERENCES

[1] Woods-Robinson, R., Han, Y., Zhang, H., Ablekim, T., Khan, I., Persson, K. A., and Zakutayev, A. (2020). Wide band gap chalcogenide semiconductors. *Chemical reviews*, **120**(**9**):4007–4055.

[2] Chen, J., Ouyang, W., Yang, W., He, J.-H., and Fang, X. (2020). Recent progress of heterojunction ultraviolet photodetectors: materials, integrations, and applications. *Advanced Functional Materials*, **30**(**16**):1909909.

[3] Yildirim, M. A., Ateş, A., and Astam, A. (2009). Annealing and light effect on structural, optical and electrical properties of CuS, CuZnS and ZnS thin films grown by the SILAR method. *Physica E: Low-dimensional Systems and Nanostructures*, **41**(**8**):1365–1372.

[4] Uhuegbu, C. and E. Babatunde. (2010). Spectral analysis of copper zinc sulphide ternary thin film grown by solution growth technique. *American Journal of Scientific and Industrial Research*, **1**(**3**):397–400.

[5] Huse, N. P., Patil, R. M., and Sharma, R. (2023). Characterization of economic and non-toxic copper doped zinc sulfide thin film grown by a facile chemical bath deposition method. *ES Materials & Manufacturing*, **20**:839.

[6] Feng, M., Zhou, H., Guo, W., Zhang, D., Ye, L., Li, W., Ma, J., Wang, G., and Chen, S. (2018). Fabrication of P-type transparent conducting $Cu_xZn_{1-x}S$ films on glass substrates with high conductivity and optical transparency. *Journal of Alloys and Compounds*, 750:750– 756.

[7] Krishna, V. G. and Mahesha, M. (2020). Characterization of transparent p-type Cu: ZnS thin films Grown by spray pyrolysis technique. *Journal of Alloys and Compounds*, **848**:156568.

[8] Najim, A., Hartiti, B., Labrim, H., Fadili, S., Tahri, M., Ertuğrul, M., Thevenin, P., and M. Mehr, F. (2022). The effect of deposition time on the growth and properties of cupper doped zinc sulfide thin Films deposited via spray pyrolysis. *Materials Chemistry and Physics*, **290**:126481.

[9] Xu, X., Shukla, S., Liu, Y., Yue, B., Bullock, J., Su, L., Li, Y., Javey, A., Fang, X., and Ager, J. W. (2018). Solution-processed transparent self-powered p-CuS-ZnS/n-ZnO UV photodiode. *physica status solidi (RRL)–Rapid Research Letters*, **12**(**2**):1700381.

[10] Ni, W.-S., Lin, Y.-J., Chang, H.-C., Liu, C.-J., and Chen, L.-R. (2015). Luminescence behavior and compensation effect on the hole concentration in the sol–gel $Zn_{1-x}Cu_xS_y$ films with different compositions. *Journal of Luminescence*, **168**:241–244.

[11] Guan, X.-H., Qu, P., Guan, X., and Wang, G.-S. (2014). Hydrothermal synthesis of hierarchical CuS/ZnS nanocomposites and their photocatalytic and microwave absorption properties. *RSC Advances*, **4**(**30**):15579–15585.

[12] Adelifard, M., Eshghi, H., and Mohagheghi, M. M. B. (2012). Synthesis and characterization of nanostructural CuS–ZnS binary compound thin films prepared by spray pyrolysis. *Optics Communications*, **285**(**21-22**):4400–4404.

[13] Sreejith, M., Deepu, D., Kartha, C. S., Rajeevkumar, K., and Vijayakumar, K. (2014). Tuning the properties of sprayed CuZnS films for fabrication of solar cell. *Applied physics letters*, **105** (**20**).

[14] Khanlary, M. R., Alizade, F., and Malekfar, R. (2020). Optical and structural investigation of ZnS: Cu thin films synthesized by spray pyrolysis. *Optical and Quantum Electronics*, **52**(**5**):237.

[15] Krishna, V. G. and Mahesha, M. (2021). n-ZnO/p-CuZnS heterostructure deposited by spray pyrolysis for photosensor application in the UV region. *Sensors and Actuators A: Physical*, **332**:113169.

[16] Diamond, A. M., Corbellini, L., Balasubramaniam, K., Chen, S., Wang, S., Matthews, T. S., Wang, L.-W., Ramesh, R., and Ager, J. W. (2012). Copper-alloyed ZnS as a p-type transparent conducting material. *physica status solidi (a)*, **209**(**11**):2101–2107.

[17] Dula, M., Yang, K., and Ichimura, M. (2012). Photochemical deposition of a p-type transparent alloy semiconductor Cu_xZn_yS. *Semiconductor Science and Technology*, **27**(**12**):125007.

[18] Ichimura, M. and Maeda, Y. (2015). Conduction type of nonstoichiometric alloy semiconductor Cu_xZn_yS deposited by the photochemical deposition method. *Thin Solid Films*, **594**:277–281.

[19] Chalana, S., Ganesan, V., and Pillai, V. M. (2015). Surface plasmon resonance in nanostructured Ag incorporated ZnS films. *AIP Advances*, **5**(**10**).

[20] Emegha, J., Olofinjana, B., Ukhurebor, K., Aigbe, U., Samuel, A., and Eleruja, M. (2022a). Effect of deposition temperature on the properties of copper-zinc sulphide thin films using mixed copper and zinc dithiocarbamate precursors. *Gazi University Journal of Science*, pages 1–1.

[21] Emegha, J. O., Olofinjana, B., Ukhurebor, K. E., Adegbite, J. T., and Eleruja, M. A. (2022b). Electrical properties of semiconducting copper zinc sulphide thin films. *Curr. Appl. Sci. Technol*, **22**(**1**):1–9.

[22] Chalana, S., Bose, R. J., Krishnan, R. R., Kavitha, V., Sreedharan, R. S., and Pillai, V. M. (2016).

Structural phase modification in Cu incorporated nanostructured zinc sulfide thin films. *Journal of Physics and Chemistry of Solids*, **95**:24–36.

[23] Sundaram, S. K., Subramanian, S., Panneerselvam, V., and Salammal, S. T. (2021). Temperature-dependent phase transition of CuZnS thin films and its effects on morphological, optical and electrical properties. *Thin Solid Films*, **733**:138810.

[24] Öztaş, M., Bedir, M., Yazici, A. N., Kafadar, E. V., and Toktamış, H. (2006). Characterization of copper-doped sprayed ZnS thin films. *Physica B: Condensed Matter*, **381**(**1-2**):40–46.

[25] Shaili, H., Salmani, E. m., Essajai, R., Beraich, M., Battal, W., Ouafi, M., Elhat, A., Rouchdi, M., Ez-Zahraouy, H., and Hassanain, N. (2021). Structural, electronic and optical properties of Cu-doped ZnS thin films deposited by the ultrasonic spray method-DFT study. *Optical and Quantum Electronics*, **53**(**6**):300.

[26] Whyte, S., Ogbuefi, U., Daniel-Mkpume, C., Anyaka, B., Okorie, B., and Ezema, F. (2020). The influence of substrate temperature on properties of zinc sulphide thin films synthesized by chemical spray pyrolysis. *Asian Journal of Basic Science & Research (AJBSR)*, **2**(**1**):01–15.

[27] Offor, P., Okorie, B., Ezema, F., Aigbodion, V., Daniel-Mkpume, C., and Omah, A. (2015). Synthesis and characterization of nanocrystalline zinc sulphide thin films by chemical spray pyrolysis. *Journal of Alloys and Compounds*, **650**:381–385.

[28] Chen, L.-C. and Hsieh, C.-A. (2015). Characterization of CuZnO diodes prepared by ultrasonic spray method. *Journal of Thermal Spray Technology*, **24**:1542–1548.

[29] Ramasamy, K., Malik, M. A., Helliwell, M., Raftery, J., and O'Brien, P. (2011). Thio-and dithio-biuret precursors for zinc sulfide, cadmium sulfide, and zinc cadmium sulfide thin films. *Chemistry of Materials*, **23**(**6**):1471–1481.

[30] Sreedhar, M., Neelakanta, R. I., Bera, P., Shyju, T., and Anandan, C. (2017). Studies of Cu-doped ZnS thin films prepared by sputtering technique. *Surface and Interface Analysis*, **49**(**4**): 284–290.

[31] Nasiri, S., Rabiei, M., Palevicius, A., Janusas, G., Vilkauskas, A., Nutalapati, V., and Monshi, A. (2023). Modified Scherrer equation to calculate crystal size by XRD with high accuracy, examples Fe_2O_3, TiO_2 and V_2O_5. *Nano Trends*, **3**:100015.

[32] Disha, S. A., Hossain, M. S., Habib, M. L., and Ahmed, S. (2024). Calculation of crystallite sizes of pure and metals doped hydroxyapatite engaging Scherrer method, Halder-Wagner method, Williamson-Hall model, and size-strain plot. *Results in Materials*, **21**:100496.

[33] Brafman, O. and Mitra, S. (1968). Raman effect in wurtzite-and zinc-blende-type ZnS single crystals. *Physical Review*, **171**(**3**):931.

[34] Ebisuzaki, Y. and Nicol, M. (1972). Raman spectrum of hexagonal zinc sulfide at high pressures. *Journal of Physics and Chemistry of Solids*, **33**(**3**):763–766.

[35] Xiong, Q., Wang, J., Reese, O., Lew, Y. V. L., and Eklund, P. (2004). Raman scattering from surface phonons in rectangular cross-sectional w-ZnS nanowires. *Nano Letters*, **4**(**10**):1991–1996.

[36] Cheng, Y., Jin, C., Gao, F., Wu, X., Zhong, W., Li, S., and Chu, P. K. (2009). Raman scattering study of zinc blende and wurtzite ZnS. *Journal of Applied Physics*, **106**(**12**).

[37] Nien, Y.-T. and Chen, I.-G. (2006). Raman scattering and electroluminescence of ZnS: Cu, Cl phosphor powder. *Applied Physics Letters*, **89**(**26**).

[38] Minceva-Sukarova, B., Najdoski, M., Grozdanov, I., and Chunnilall, C. (1997). Raman spectra of thin solid films of some metal sulfides. *Journal of molecular structure*, **410**:267–270.

[39] Hussain, S., Lalla, N., Kuo, Y.-K., Lakhani, A., Sathe, V., Deshpande, U., and Okram, G. (2018). Thermoelectric properties of Ag-doped CuS nanocomposites synthesized by a facile polyol method. *Physical Chemistry Chemical Physics*, **20**(**8**):5926–5935.

[40] Enriquez, J. P. (2013). Effect of annealing time and temperature on structural, optical and electrical properties of CdS films deposited by CBD. *Chalcogenide Letters*, **10**(**2**).

[41] Pankove, J. I. (1975). *Optical processes in semiconductors*. Courier Corporation.

[42] Patel, S. P., Pivin, J., Kumar, V. S., Tripathi, A., Kanjilal, D., and Kumar, L. (2010). Grain growth and structural transformation in ZnS nanocrystalline thin films. *Vacuum*, **85**(**2**):307–311.

[43] AL-Diabat, A. M., Ahmed, N. M., Hashim, M., Chahrour, K. M., and Bououdina, M. (2016). Effect of deposition temperature on structural and optical properties of chemically sprayed ZnS thin films. *Procedia Chemistry*, **19**:485–491.

[44] Brown, M. and Jakeman, E. (1966). Theory of the four-point probe technique as applied to the measurement of the conductivity of thin layers on conducting substrates. *British Journal of Applied Physics*, **17**(**9**):1143.

[45] Agumba, O. J. (2010). Design and fabrication of a simple four-point probe system for electrical characterization of thin films. Master's thesis, Kenyatta University, Kenya.

[46] Mugwang'a, F., Karimi, P., Njoroge, W., and Omayio,

O. (2015). Characterization of aluminum doped zinc oxide (AZO) thin films prepared by reactive thermal evaporation for solar cell applications. *Journal of Fundamentals of Renewable Energy and Applications*, **5**(**4**):1000170–1000175.

[47] Tareq, S. (2021). *The optical and electrical characteristics of ZnO/MoS2 transparent oxide composite films*. PhD thesis, Kadir Has University.

[48] Rockett, A. (2007). *The materials science of semiconductors*. Springer Science & Business Media.

APPENDIX

Table 1: Cu doping percentage and average sheet resistance grown at about 420 °C.

Cu doping percentage (at. %)	Average sheet resistance (MΩ)
0	121.703
4	23.981
8	12.541
12	10.903
16	0.827
20	0.028

Table 2: Density of dislocation at different substrate temperatures.

Substrate temperature (°C)	D(nm)	$\sigma \times 10^{16}$(lines/m^2)
380	4.427	5.103
410	3.443	8.436

Table 3: Strain in the thin films synthesised at 380 °C and 410 °C substrate temperatures.

Peak position (2θ)		β (10^{-2} radian)		ε ×10^{-2}	
380	410	380	410	380	410
25.38	25.50	3.94	8.33	4.38	9.20
31.18	31.18	3.46	4.67	3.10	4.19
34.23	34.64	5.33	4.13	4.33	3.31
42.23	39.77	3.77	2.87	2.44	1.99
51.29	50.52	6.97	3.64	3.63	1.93
	59.31		1.86		0.82
	61.75		3.85		1.61
Average ε				3.58	3.29

Table 4: Raman peaks of the synthesised CuZnS thin films at different substrate temperatures.

Substrate temperatures °C	peak position (cm^{-1})
380	269, 315, 349, 542, 400, 431, 473, 540, 614, 690, 761
410	270, 305, 350, 389, 473, 562, 675, 741

Table 5: EDX analysis report about the binary oxides in the deposited thin film.

Analyte	Result	
SiO2	86.080	%
CaO	8.841	%
K2O	2.954	%
SO3	1.434	%
ZnO	0.311	%
Cl	0.292	%
CuO	0.090	%

Table 6: Bandgap, and Urbach energies at different substrate temperatures.

Substrate temperature (°C)	Band gap, Eg (eV)	Sub-band gap, Eg (eV)	Urbach energy, Eu (eV)
380	3.43	3.14	0.934
410	3.40	3.10	1.159

Table 7: Electrical conductivity at different substrate temperatures.

Substrate temperature (°C)	Thin film thickness (nm)	Resistivity Ωcm	Conductivity $(\Omega cm)^{-1}$
380	841.67	1936.82	5.16×10^{-4}
410	755.33	125.93	7.94×10^{-3}